

See discussions, stats, and author profiles for this publication at: <https://www.researchgate.net/publication/230847782>

# Self-Assembly of Filamentous Amelogenin Requires Calcium and Phosphate: From Dimers via Nanoribbons to Fibrils

ARTICLE in BIOMACROMOLECULES · SEPTEMBER 2012

Impact Factor: 5.75 · DOI: 10.1021/bm300942c · Source: PubMed

---

CITATIONS

10

READS

50

## 9 AUTHORS, INCLUDING:



[Yifan Cheng](#)

University of California, San Francisco

96 PUBLICATIONS 5,204 CITATIONS

[SEE PROFILE](#)



[Feroz Khan](#)

University of California, San Francisco

15 PUBLICATIONS 135 CITATIONS

[SEE PROFILE](#)



[Jeremy A Horst](#)

University of California, San Francisco

26 PUBLICATIONS 242 CITATIONS

[SEE PROFILE](#)



[Stefan Habelitz](#)

University of California, San Francisco

114 PUBLICATIONS 2,529 CITATIONS

[SEE PROFILE](#)

**Self-assembly of Filamentous Amelogenin Requires Calcium and Phosphate: From Dimers via Nanoribbons to Fibrils**

Journal:	<i>Biomacromolecules</i>
Manuscript ID:	bm-2012-00942c.R1
Manuscript Type:	Article
Date Submitted by the Author:	n/a
Complete List of Authors:	Martinez-Avila, Olga; University of California, Preventive and Restorative Dental Sciences Wu, Sheping; University of California, Biochemistry & Biophysics Kim, Seung Joong; University of California, Bioengineering and Therapeutic Sciences Cheng, Yifan; UCSF, Samudrala, Ram; University of Washington, Microbiology Khan, Feroz; University of California, Preventive and Restorative Dental Sciences Sali, Andrej; University of California, Bioengineering and Therapeutic Sciences Horst, Jeremy; University of California, Bioengineering and Therapeutic Sciences Habelitz, Stefan; University of California, Department of Preventive and Restorative Dental Sciences

SCHOLARONE™  
Manuscripts

1  
2  
3     **Self-assembly of Filamentous Amelogenin Requires Calcium and Phosphate: From Dimers**  
4         **via Nanoribbons to Fibrils**  
5  
6  
7

8     Olga Martinez-Avila<sup>1</sup>, Shenping Wu<sup>2</sup>, Seung Joong Kim<sup>3</sup>, Yifan Chen<sup>2</sup>, Feroz Khan<sup>1</sup>,  
9  
10    Ram Samudrala<sup>4</sup>, Andrej Sali<sup>3</sup>, Jeremy A. Horst<sup>5</sup>, Stefan Habelitz<sup>1\*</sup>  
11  
12  
13  
14

15         <sup>1</sup>Department of Preventative and Restorative Dental Sciences,  
16  
17         707 Parnassus Ave., San Francisco, CA 94143,  
18  
19             University of California  
20  
21

22         <sup>2</sup>Department of Biochemistry & Biophysics,  
23  
24         600 16th Street, Room S312B, San Francisco, CA 94158  
25  
26             University of California  
27  
28

29         <sup>3</sup>Department of Bioengineering and Therapeutic Sciences, Department of Pharmaceutical  
30  
31             Chemistry, and California Institute for Quantitative Biosciences,  
32  
33         Byers Hall Room 503B, 1700 4th Street, San Francisco, CA 94158  
34  
35             University of California  
36  
37

38         <sup>4</sup>Department of Microbiology, 208 Rosen Building, Box 357735 · Seattle WA 98195  
39  
40             University of Washington  
41  
42

43         <sup>5</sup>Department of Orofacial Sciences, 513 Parnassus Ave. San Francisco, CA 94143  
44  
45             University of California  
46  
47  
48  
49  
50

51         \*Corresponding author:  
52  
53  
54

55         Stefan Habelitz, phone: 1-415-514-0818; email: Stefan.habelitz@ucsf.edu  
56  
57  
58  
59  
60

## ABSTRACT

Enamel matrix self-assembly has long been suggested as the driving force behind aligned nanofibrous hydroxyapatite formation. We tested if amelogenin, the main enamel matrix protein, can self-assemble into ribbon-like structures in physiologic solutions. Ribbons 17nm wide were observed to grow several microns in length, requiring calcium, phosphate, and pH 4.0-6.0. The pH range suggests that the formation of ion bridges through protonated histidine residues is essential to self-assembly, supported by a statistical analysis of 212 phosphate-binding proteins predicting twelve phosphate-binding histidines. Thermophoretic analysis verified the importance of calcium and phosphate in self-assembly. X-ray scattering characterized amelogenin dimers with dimensions fitting the cross-section of the amelogenin ribbon, leading to the hypothesis that antiparallel dimers are the building blocks of the ribbons. Over 5-7 days, ribbons self-organized into bundles composed of aligned ribbons mimicking the structure of enamel crystallites in enamel rods. These observations confirm reports of filamentous organic components in developing enamel and provide a new model for matrix-templated enamel mineralization.

**KEYWORS:** Enamel, amelogenin, self-assembly, protonated histidine, biominerlization

## INTRODUCTION

Self-assembly of extracellular matrix proteins results in key biological structural materials, such as collagens, keratins, and cellulose, which cells use to build entire tissues and organs<sup>1, 2</sup>. The formation of dental enamel differs from this general concept as the fully developed tissue is basically free of the original organic matrix and made of 95% mineral, crystalline carbonated hydroxyapatite rendering a clear relationship between the structure of organic and inorganic components difficult. In mammalian and marsupial enamel, extremely thin (50 nm diameter) apatite fibers of several hundreds of micrometer length are packed into rods or prisms of about 5  $\mu\text{m}$  width<sup>3</sup>. Enamel rods have species specific organization and alignment and are often separated by interrod enamel, also composed of aligned apatite nanofibers decussating enamel rods at an angle of about 60°<sup>4</sup>. The remarkable architectures of enamel structures suggest that a precise mechanism must have evolved that facilitated control over apatite crystallization at the nanometer length scale. The enamel matrix is generated by ameloblasts which may have an important role in organizing matrix proteins and apatite crystallites, but at the nanometer length scale it is conceivable that the matrix itself orchestrates the mineralization events and controls nucleation, growth rate, morphology and direction of growth of calcium phosphate mineral<sup>5-8</sup>. However, up to this date the role and the molecular mechanisms of the developing enamel matrix in synthesizing the unique architecture of mineralized enamel remain unclear.

Amelogenin proteins comprise about 90% of the organic matrix and are crucial for functional enamel development by orchestrating the mineralization of apatite crystals as shown in amelogenin deficient mice<sup>7</sup>. Self-assembly of amelogenin has been proposed to be critical for shaping the morphology and alignment of the growing apatite crystals<sup>9, 10</sup>. The human full-

length amelogenin (H175) consists of 175 amino acid residues and is predominantly hydrophobic with a hydrophilic C-terminus of about 12 residues. Many structural motifs have been attributed to this protein. The molecule is intrinsically disordered in its monomeric state, but polyproline,  $\beta$ -turn and  $\beta$ -sheet like, as well  $\alpha$ -helical elements have been reported in assembled, nanospherical structures<sup>11-15</sup>. Due to its hydrophobic nature, the full-length amelogenin protein has a high propensity to aggregate in aqueous solutions around its isoelectric point of 6.8<sup>16</sup>. The formation of 20 to 60 nm wide nanospheres and oblates has been described in numerous studies<sup>17</sup>. A model which includes the formation of chain-like aggregates with the amelogenin nanosphere as building block has been developed to explain the protein's ability to generate aligned apatite nanocrystals in enamel which almost exclusively grow along their crystallographic c-axis<sup>14, 17-20</sup>.

Previous structural studies, however, paid little attention to the effect of both calcium and phosphate ions on protein self-assembly. Amelogenin's structural development has been largely investigated in the absence of these ions or as a function of only calcium or only phosphate<sup>9, 11, 17, 21</sup>. In addition previous studies were performed with the assumption that amelogenin assembles within seconds or minutes. While this may be true for short peptides, proteins in general require several hours or days to form supramolecular structures<sup>9, 11, 22, 23</sup>. In recent studies our group took these factors into consideration as well as the amphiphilic nature of amelogenin's primary structure and developed a water-in-oil emulsion system that produced novel self-assembled structures of amelogenin. In the emulsion system amelogenin molecules stretched along the surface of micelles and were thus able to interact between the hydrophobic N-termini and facilitating the formation of nanoribbons and nanohelices<sup>24, 25</sup>. Nanoribbons formed at pHs between 4 and 7.5, aligned themselves, forming bundles of several micrometer width, indicating

1  
2  
3 that the protein itself has the capacity to form a structure similar to the mineral crystallites in  
4 mature enamel suggesting it may be a suitable template for guiding apatite crystallization<sup>25</sup>.  
5  
6

7 Based on these findings in an artificial system, we now further investigated the role of calcium  
8 and phosphate on self-assembly in an oil-free, aqueous environment. By careful analysis of the  
9 effect of pH on amelogenin supramolecular structure, we developed a procedure that facilitated  
10 the synthesis of amelogenin nanoribbons and under aqueous and physiological conditions. Our  
11 new model of amelogenin self-assembly is supported by a functional residue signature analysis  
12 demonstrating the high probability of phosphate binding to histidine. Furthermore, *ab-initio*  
13 shape calculations from Small Angle X-ray Scattering (SAXS) data demonstrate the formation of  
14 amelogenin dimers which may act as building blocks for the hierarchical assembly of  
15 amelogenin nanoribbons and fibrils.  
16  
17  
18  
19  
20  
21  
22  
23  
24  
25  
26  
27  
28  
29  
30

## EXPERIMENTAL SECTION

31  
32  
33  
34 **Expression and purification of amelogenin.** Recombinant human amelogenin rH174 and  
35 cleavage product rH146 were expressed in BL21DE3 plysS *Escherichia coli* and purified on C4  
36 hydrophobic beads as previously described<sup>26</sup>. The purity of the protein batches was above 95%  
37 as assessed by HPLC. MMP-20 proteolytic product rH146 lacks 28 amino acids at the C-  
38 terminus. Recombinant amelogenin also lacks the first residue (Met) compared to the native  
39 human full-length protein H175.  
40  
41  
42  
43  
44  
45

46 **Self-assembly experiments.** Lyophilized proteins were dissolved in double deionized water to  
47 prepare protein stock solutions at concentration of 4-6 mg/mL. Calcium and phosphate stock  
48 solutions were prepared using reagent grade chemicals CaCl<sub>2</sub> (133.6 mM) and KH<sub>2</sub>PO<sub>4</sub> (83.6  
49 mM) and filtered (0.22 µm). Suspensions of 500µL total volume containing 0.4, 0.8, 1.2, 1.6 or  
50 2.0 mg/mL of amelogenin rH174 were prepared by adding KH<sub>2</sub>PO<sub>4</sub> in one test tube containing  
51 rH174 and CaCl<sub>2</sub> in another one with same amount of rH174. Both tubes were combined  
52 resulting in final concentrations of 0, 3.3 or 33.4 mM of CaCl<sub>2</sub> and 0, 2.1 or 20.9 mM of KH<sub>2</sub>PO<sub>4</sub>  
53  
54  
55  
56  
57  
58  
59  
60

1  
2  
3 and vortexed for about 30 s. The pH of resulting CaP protein solutions was initially around 2 due  
4 to residual TFA<sup>19</sup>. The solution was then adjusted to specific pH 3, 4.0, 4.5, 5.1, 5.5, 6.0, 6.5,  
5  
6 7.0, 7.4 or 8.0 ( $\pm 0.1$ ) by adding KOH. Emphasis on pH between 4 and 6 was placed because  
7 previous studies on emulsions showed higher propensity to ribbon formation at these pH<sup>24, 25</sup>. In  
8 addition, at pH below 6, histidine residues will protonate which may have significant influence  
9 on protein-protein and protein-mineral interactions. Protein solutions were incubated at 37 °C for  
10 up to 7 days. All samples prepared in triplicates. A volume of 2-15 µL of suspensions was  
11 extracted at different time points and prepared for a full characterization by the methods listed  
12 below<sup>19</sup>.  
13  
14  
15  
16  
17  
18  
19  
20

21 **Atomic force microscopy.** Extracts (15 µL) were pipetted onto microscope glass slides and kept  
22 for 1 h in a wet cell to immobilize products onto glass slide avoiding evaporation. Subsequently,  
23 samples were washed off with 1-2 drops of double deionized water, immediately dried with dust-  
24 free canned air. AFM was performed in dry conditions using tapping mode with a Nanoscope III  
25 (Digital Instruments, Santa Barbara, CA, USA) and Si-cantilevers (SSS-NCH, Nanoworld,  
26 Neuchâtel, Switzerland). The length and height of ribbons were measured from the AFM height-  
27 mode images using Nanoscope V512.r3 software and an average value determined from 50  
28 points per sample group.  
29  
30  
31  
32  
33  
34

35  
36  
37 **Transmission electron microscopy.** As described previously<sup>25</sup>, a 2.0 µL drop of sample  
38 solution was adsorbed for 60 s to a glow-discharged carbon-coated copper grid (Ted Pella,  
39 Redding, CA, USA) washed off with two drops of double deionized water and air-dried. For  
40 negative staining, the TEM grid was stained with a 2% methylamine tungstate solution, pH 6.8,  
41 (NANO-W; Yaphank, NY, USA) after being washed off by two drops of water. Grids were  
42 imaged with an FEI Tenai T12 TEM (FEI company, Hillsboro, OR, USA) at 120 kV. Data were  
43 acquired with a 4 k by 4 k Gatan UltraScan CCD camera (Gatan, Pleasanton, CA, USA).  
44  
45  
46  
47  
48  
49  
50

51 **Small-angle X-Ray scattering.** SAXS experiments were performed with the intention to detect  
52 the small units/particles in the suspension and to determine their size as a function of increasing  
53 pH in order to obtain information on possible building blocks of the nanoribbons. Protein stocks  
54 and corresponding buffers were mixed as described above at final protein concentrations of 2.0,  
55  
56  
57  
58  
59  
60

1  
2  
3 1.5, 1.0, 0.5, 0.25 and 0.1 mg/mL. The latter two concentrations were too diluted and did not  
4 provide sufficient scattering. In contrast, scattering was too strong when unfiltered suspensions  
5 were used, indicating the presence of high numbers of micrometer sized particles. The  
6 suspensions were therefore filtered through 0.1  $\mu$ m membranes (Millipore, Bedford, MA).  
7  
8 Protein content of the 2.0 mg/ml samples was analyzed before and after filtering using Bradford  
9 Protein Assay. Highly acidic solutions will promote monomer formation due to increased surface  
10 charges of the protein<sup>16</sup>. A sequential increase in pH towards neutral pH will allow us to follow  
11 the aggregation behavior of the proteins. The pH was adjusted to 1.5 (addition of HCl), 3.7, 5.6  
12 or 7.5 (addition of KOH) in 3.3 mM of CaCl<sub>2</sub> and 2.1 mM of KH<sub>2</sub>PO<sub>4</sub>. SAXS measurements of  
13 rH174 and rH146 were carried out at Beam line 4-2 of the Stanford Synchrotron Radiation  
14 Lightsource. All SAXS profiles were collected at 15 °C after 24 to 48 hours of sample  
15 preparation and incubation at 37 °C. Suitable spectra were obtained at multiple concentrations  
16 from 0.5 to 2 mg/mL. 5% glycerol was added to reduce radiation damage. Controls without  
17 protein but 5% glycerol were also analyzed<sup>27</sup>.  
18  
19  
20  
21  
22  
23  
24  
25  
26  
27

28  
29  
30 **Modeling.** The *ab-initio* shapes of amelogenin (rH146 and rH174) monomers and dimers were  
31 initially calculated from a merged experimental SAXS profile by running DAMMIF 20 times  
32 and refined with additional 50 DAMMIN runs<sup>28</sup>, followed by superposition and averaging with  
33 DAMAVER<sup>29</sup>. Fitting of *ab-initio* shapes into the TEM images was visualized by customized  
34 scripts in UCSF Chimera<sup>30</sup>.  
35  
36  
37  
38

39  
40 **Meta-Functional Signature.** A meta-functional signature (MFS<sup>31</sup>) compilation was built to  
41 estimate the probability for each residue in a given protein to bind soluble phosphate ions  
42 (mfsPO<sub>4</sub>), as was done previously for calcium binding<sup>32</sup>. Nonlocal contact predictions were  
43 combined with one dimensional predictions of conservation and structural features, by training a  
44 logistic regression to maximize scores for 591 phosphate binding among 39,641 residues in 190  
45 proteins. Proteins were selected from all crystal diffraction structures in the Protein Databank  
46<sup>33</sup> [accessed May 10<sup>th</sup>, 2010] by presence of a phosphate ion noncovalently bound to the side  
47 chains of at least two residues (within a half Ångstrom of van der Waals distance). The set was  
48 filtered for non-redundancy by starting with the highest resolution (<2.1 Å) structures and  
49 progressively adding proteins to maximize diversity and maintain <30% sequence identity.  
50  
51  
52  
53  
54  
55  
56  
57  
58  
59  
60

A ten-fold cross validation benchmark experiment was performed to assess the accuracy of the mfsPO4 methodology. PO4-binding residues were considered positive instances and all other residues were considered negative instances for training in a logistic regression of sequence-derived structural features, as described previously<sup>31</sup>. The 212 proteins were randomly distributed into ten 10% subsets. Each subset of proteins was used to test the accuracy of the mfsPO4 method when trained on the remaining 90%. Ten regressions were constructed, each with an input data set of 191 or 190 proteins (4/5 shared with the other sets), and tested on the 21 or 22 proteins not included in the input set. Since no protein was tested more than once, each test is independent and analyses can be graphed together. Depiction of performance is illustrated by a precision recall plot. The regression trained on all 212 proteins (mfsPO4) and the mfsCa method described previously<sup>32</sup> were applied to the H175 amelogenin sequence. The methods were applied to 1000 proteins which are not known to bind phosphate or calcium ions. Scores of three standard deviations above the mean for these nonbinding proteins defined the threshold for binding predictions.

**Microscale Thermophoresis (MST).** Thermophoresis was used to measure the binding interactions between labeled and unlabelled rH174 molecules using a Monolith NT.115 (NanoTemper Technologies GmbH, Munich, Germany)<sup>34</sup>. Amelogenin rH174 was labeled with a red fluorescent dye (Monolith NT<sup>TM</sup>) that uses N-Hydroxysuccinimide (NHS)- ester. Free dye was removed by purification on a Sephadex G-25 column and the labeled protein was suspended in double deionized water and freeze dried, then resuspended in acetonitrile 30% - 0.1 trifluoroacetic acid, freeze dried. Protein was then dissolved in reaction buffer at pH 2 containing 33.4 mM of CaCl<sub>2</sub> and 20.9 mM of KH<sub>2</sub>PO<sub>4</sub>. pH was adjusted to pH values of 2, 4.5 or 5.6. Control experiments were carried out under the same buffer conditions in the absence of CaP. For each binding assay, the concentration of the labeled rH174 is kept constant at 30 nM (1 $\mu$ g/ml), whereas unlabeled rH174 was titrated in a set of serial dilutions from the nanomolar to the submillimolar (100  $\mu$ M  $\approx$  2mg/ml) range.

## Results

In this study, we followed the development of self-assembled structures of amelogenin rH174 in solutions with and without calcium and phosphate ions at pH between 2 and 8 over a period of 7 days, using TEM and AFM analyses. Initially the characteristic spherical assemblies of amelogenin varying in size between 10 and 25 nm were observed (Figure 1A)<sup>9</sup>. In the absence of calcium and phosphate ions, amelogenin nanospheres were stable, though they tended to become more heterogeneous in size over time, spanning diameters of 10 to 50 nm (Figure 1B). In agreement with previous studies we observed on rare occasions that nanospheres lined up to form chains of spheres (data not shown)<sup>18</sup>. The structural development of amelogenin assemblies was severely altered when 3.3 or 33.4 mM calcium chloride and 2.1 or 20.9 mM potassium phosphate were added to the amelogenin suspensions in the pH-range of 4.0 to 6.0. At pH 4.5, low numbers of amelogenin nanospheres were initially observed at 24 hours of incubation, non-homogeneously distributed over the TEM grid. During this time period short ribbons developed occasionally and both ribbons and spheres were observed by TEM (Figure 1C). With continued incubation nanospheres completely disappeared while the numbers of nanoribbons increased. At day 3, nanoribbons were the only protein structure observed (Figure 1D). Most of the ribbons were still short with an average length of about 250 nm, including ribbons up to 800 nm long. At day 5, ribbons became more organized and domains of groups of ribbons in the parallel orientation became evident (Figure 1E). After 7 days, ribbons had formed larger aggregates that resembled fibrils or bundles (Figures. 1, F and G). These bundles measured between 500 nm and 2  $\mu$ m in width and reached several micrometers in length consisting of continuous ribbons in parallel alignment. The bundles were surrounded by shorter segments of ribbons that appeared to be in the process of being added, thus elongating the ribbons (Figure 1H, inlet of 1G) as suggested in our previous study using an oil-water system<sup>25</sup>.

When either phosphate (20.9 or 2.1mM) or calcium (33.4 or 3.3 mM) were added to the protein suspensions individually but not combined, no ribbons were observed within 7 days of incubation. Instead spherical and not well defined aggregates developed over time (Figure S1 B and C).

The importance of calcium ions for self-assembly was illustrated when EDTA was added to suspensions that contained amelogenin ribbons (Figure 1I). Ribbons disintegrated after EDTA exposure for 2 h, while nanospheres of about 20 nm diameters developed, indicating that the removal of calcium destabilizes the ribbon structure and promotes nanosphere formation.

Ribbon formation was examined as a function of *pH* for samples incubated for 7 days at concentrations of 0.4 mg/mL rH174. The lowest *pH* at which ribbons self-assembled was *pH* 4.0, producing short ribbons of 200 to 500 nm length with weak alignment (Figure 2A). At day 7, ribbons and bundles of aligned ribbons were observed at *pH* 4.5, 5.1 (not shown), 5.6 and 6.0 (Figure 2, B and C). Ribbons were absent at acidic *pH* of 2.0 and 3.0 and mainly showed a diffuse protein mass without any defined structural features (Figure S1C). At *pH* 7.0, 7.4, and 8.0, a significant amount of calcium phosphate mineral formed, rendering the observation of amelogenin supramolecular structures more difficult (Figure. S1D). There is currently no evidence that amelogenin nanoribbons also form at these *pH*s under the experimental conditions used. Figures 2D and E are AFM images of amelogenin ribbons immobilized on a glass slide before and after immersion into an aqueous solution at *pH* 2. Ribbons disintegrated into short segments of about 30 nm length within 1 min of acid exposure. In contrast, when immobilized ribbons were immersed into aqueous calcium phosphate solutions at *pH* 7.0 to 8.0, nanoribbons

1  
2  
3 did not disintegrate and remained stable for the 3-day time period studied (Figure 2F). For  
4 protein concentration of 0.4 mg/mL, kinetics of ribbon formation was enhanced in the pH range  
5 of 4.5 to 6.0, with ribbons forming within 24 hours and bundles of ribbons appearing as early as  
6 7 days. AFM measurements determined the thickness of ribbons to be 3.4 ( $\pm 0.6$ ) nm.  
7  
8  
9  
10  
11  
12  
13  
14

15 In general organization into bundles of aligned nanoribbons was accelerated with increasing  
16 amelogenin rH174 concentration. Figure 3 shows a series of TEM micrographs of amelogenin  
17 supramolecular structures obtained after 6 days of incubation in calcium phosphate solutions at  
18 37°C. For a concentration of 0.4 mg/mL, short nanoribbons were observed at low density (Figure  
19 3A). Ribbon length, number density and their parallel alignment were elevated when 0.8 mg/mL  
20 were used (Figure 3B). At a concentration of 1.2 mg/mL, formation of bundles of ribbons was  
21 observed (Figure 3C), while large numbers of amelogenin bundles consisting of aligned ribbons  
22 had developed when concentrations of 1.6 mg/mL were used (Figure 3D). Amelogenin  
23 concentration plays a significant role in the kinetics of ribbon formation, suggesting that at  
24 concentrations comparable to the developing enamel matrix (~300 mg/mL) self-assembly might  
25 occur at much faster time-scales<sup>5</sup>.  
26  
27  
28  
29  
30  
31  
32  
33  
34  
35  
36  
37  
38  
39  
40  
41  
42

43 Microscale thermophoresis (MST) experiments<sup>35</sup> were conducted with emphasis on the  
44 significance of calcium and phosphate ions for protein-protein interactions at pH 4.5 by titrating  
45 unlabeled rH174 into suspensions containing fluorescence-labeled rH174. We observed a strong  
46 change in fluorescence intensity following a sigmoidal profile when unlabeled rH174 was added  
47 in the presence of calcium and phosphate, characteristic of strong protein-protein interactions  
48 (Figure 4A). The half maximal effective concentration (EC50) was 176 nM and a dissociation  
49  
50  
51  
52  
53  
54  
55  
56  
57  
58  
59  
60

constant of  $145 \pm 12.2$  nM was determined for amelogenin interactions, corresponding to a 5 to 10-fold increased affinity compared to calcium dependent self-assembling systems, such as binding of cartilage oligomeric matrix protein to collagen<sup>36</sup>, EcoRV endonuclease binding to DNA<sup>37</sup>, or calmodulin protein binding to HIV<sup>38</sup>. In contrast, little fluorescence activity was observed in the absence of calcium and phosphate (Figure 4A), indicating that primarily non-specific interactions occurred as characteristic for protein aggregation events<sup>34, 35</sup>.

The pH dependence of ribbon formation suggests that self-assembly is linked to protonation of a functional moiety. The most likely amino acid residue that changes protonation state in the physiological pH range is histidine ( $pK_a$  6.0-6.5)<sup>39</sup>. The dependence of self-assembly upon ions indicates a functional interaction between histidine and phosphate or calcium. An earlier analysis of a 30% non-redundant set of 336 calcium-bound protein structures showed that histidine only represents 7 of 696 calcium-binding residues<sup>32</sup>. Here, we repeated this analysis for a similar set of 212 phosphate-bound protein structures, and found 132 of 950 phosphate-binding residues to be histidine, second only to arginine (Figure S3). Further, by training a meta-functional signature protocol<sup>31 32</sup> to these proteins, we were able to predict the following phosphate-binding residues in amelogenin with high confidence: 6H, 9H, 30R, 46H, 47H, 54S, 57H, 66H, 67H, 68H, 91H, 98H, 99H, 159T, 170K, 171R, 172E, 173E, 175D. Similarly, the meta-functional signature protocol trained on calcium binding sites predicts specific amelogenin residues to carry out functional interactions with calcium: including glutamic (E) and aspartic (D) acids 18E, 39E, 157D, 161E, 168D, 172E, 173E, and 175D. Figure 4B illustrates the

1  
2  
3 probability for each residue in human full-length amelogenin H175 to bind to calcium or  
4 phosphate.  
5  
6  
7  
8  
9

10 To assess the size and morphology of amelogenin particles during early stages of assembly,  
11  
12 Small Angle X-ray Scattering (SAXS) profiles (Figure S2) were obtained from filtered  
13 suspensions at pH between 1.5 and 7.5, with or without calcium and phosphate. The protein  
14 concentration decreased by about 10% for pH 1.5 and 2.5, by 31% for pH 5.6 and by 38% for pH  
15  
16 7.4. Oligomeric status was estimated from the radius of gyration ( $R_g$ ), maximum dimension  
17 (D<sub>max</sub>) (Table S1), radial distribution functions (Figure S2), and mass calculations <sup>40</sup>. For the  
18 full-length human amelogenin (rH174), monomers were observed consistently at pH 1.5 (R<sub>g</sub>  
19  
20 46.4 Å, D<sub>max</sub> 158 Å). When both calcium and phosphate were present, particle size, as measured  
21 by R<sub>g</sub> increased continuously until pH 5.6, whereupon it matched the expected dimensions and  
22 (D<sub>max</sub>) (Table S1), radial distribution functions (Figure S2), and mass calculations <sup>40</sup>. For the  
23 full-length human amelogenin (rH174), monomers were observed consistently at pH 1.5 (R<sub>g</sub>  
24 46.4 Å, D<sub>max</sub> 158 Å). When both calcium and phosphate were present, particle size, as measured  
25 by R<sub>g</sub> increased continuously until pH 5.6, whereupon it matched the expected dimensions and  
26 mass of a dimer (R<sub>g</sub> 64.1 Å, D<sub>max</sub> 209 Å). We observed similar behavior for the C-terminal  
27 truncated human amelogenin fragment (rH146) which lacks the 28 C-terminal amino acid  
28 residues of rH174, transitioning from a monomer at pH 1.5 (R<sub>g</sub> 37.2 Å, D<sub>max</sub> 130 Å) to a dimer at  
29 pH 5.6 (R<sub>g</sub> 51.6 Å, D<sub>max</sub> 146 Å), in agreement with dimensions determined by SAXS on the 20 kd  
30 native porcine amelogenin <sup>41</sup>. In agreement with light scattering data by others <sup>42</sup>, rH174 and  
31 rH146 monomers were much more abundant than dimers in the absence of calcium and  
32 phosphate regardless of the pH (Figures S2 E, F). Dimerization in the absence of calcium  
33 phosphate may also be reduced due to the low ionic strength of the solution which reduces the  
34 aggregation propensity of amelogenin <sup>43</sup>.  
35  
36  
37  
38  
39  
40  
41  
42  
43  
44  
45  
46  
47  
48  
49  
50  
51  
52  
53  
54  
55  
56  
57  
58  
59  
60

In order to construct a low-resolution model of protein structures from SAXS data, *ab-initio* shape reconstructions were performed on data obtained at pH 1.5 (monomers) and at pH 5.6 (dimers) of rH174 in the presence of calcium and phosphate (Figure 5A). Superposition of two rH174 monomers into an rH174 dimer model revealed a reasonably good fit (ccc: 0.82) when the two monomers were allowed to overlap by three quarters of their lengths in antiparallel orientation (Figure 5B). Similarly, superposition of two rH146 monomers at pH 1.5 into the rH146 dimer at pH 5.6 resulted in a slightly better fit (ccc: 0.84). We like to point out that SAXS data alone does not define the secondary structure of amelogenin.

Prevalence of  $\beta$ -sheets in these ribbons was observed by Raman-spectroscopy previously<sup>25</sup>, but the presented structural model of Fig. 5 is a low-resolution model and does not include information on secondary structure of amelogenin. The nanoribbon structural model takes into consideration structural information from TEM observations and measurements on ribbons made from rH174 and from rH146 further reinforces some elements of this model, like the antiparallel orientation of amelogenin molecules and the lateral C-terminal position in the dimer. We have previously produced nanoribbon assemblies of truncated amelogenin rH146 in an emulsion system<sup>24</sup> and were also able to produce ribbons of rH146 without the use of an oil phase by procedures very similar to the ones described in this study for rH174. Nanoribbons of rH146 (Fig. S5), do not grow to the length of rH174 ribbons and do not show parallel alignment. Importantly for the model, the width of ribbons from rH146 was 148 ( $\pm 7$ ) Å and was significantly reduced compared to those of rH174 (167 ( $\pm 10$ ) Å). Therefore we hypothesize that the C-terminus is not part of the overlap zone and is instead oriented towards the ribbon edges in an antiparallel arrangement of the monomers (Fig. 5C). The location of the C-terminus in the assembly is

further supported by the shorter superimposed SAXS-based shape of the rH146 dimer compared to rH174 dimer at pH 5.6 (ccc: 0.76), demonstrating that the 28 residues missing in the rH146 construct are associated with the non-overlapping region in the dimer. A side view of the nanoribbon assembly shows the interdigitated arrangement of the dimers within the structure (Fig. 5D).

The proposed models of the rH174 dimer (Fig. 5) were superimposed onto a nanoribbon visualized by TEM and restricted to the 30 Å height determined by AFM<sup>25</sup>. The apparent repeating units shown by TEM relatively good fit with the size and shape of the SAXS dimer model (Fig. 6). The axial symmetry of the repeating units limits the possible rotational positions of the dimer, thereby defining the interfacial surfaces on the SAXS-based dimer and monomer models. The maximum length of the rH174 dimer is ~40 Å longer than the width of the rH174 ribbon measured by TEM, while the maximum diameter of the rH146 dimer matches very well the width of the rH146 ribbon in TEM (Table S1). This finding indicates a conformational shift and inward folding of C-terminal residues upon self-assembly (Fig. 6).

### Discussion

Self-assembly is a process in which a disordered system forms an organized, well-defined structure or pattern as a consequence of specific, local interactions among the components themselves, without external direction and differs from disorganized aggregation, random assembly, precipitation or deposition. It requires the formation of building blocks or units with specific structural motifs which are able to form residue specific non-covalent bonds generating a systematic arrangement of these units resulting in unique structures at the nanometer to

micrometer length scale. This study shows that the recombinant full-length human amelogenin protein, rH174, can self-assemble into self-aligning nanoribbons and form bundles consisting of aligned amelogenin ribbons in calcium phosphate solutions. The amelogenin structures generated in this study under aqueous conditions were identical to the ones developed in metastable water in oil emulsion<sup>25</sup>. While in the emulsion system the alignment of amelogenin molecules along the oil-water interface was critical to prevent a hydrophobic collapse, in this study the pH shift and the presence of calcium and phosphate were sufficient to stabilize the protein backbone. In the oil-water system, nanoribbons formed at pH between 4 and 7.4. In contrast, under aqueous conditions nanoribbons only formed at pH between 4.0 and 6.0 indicating that protonation of histidine may be required for intermolecular interactions. While this pH range is lower than what has been described for the liquid phase of secretory enamel<sup>44, 45</sup>, it is in the range of the pH widely reported for exocytic vesicles (pH 5.0-6.0)<sup>46</sup>. Hence dimerization of amelogenin may already occur before exocytosis. Since TEM analysis of vesicles in ameloblasts does not indicate the presence of larger filamentous entities<sup>47</sup>, nanoribbon assembly is more likely to occur in the extracellular space which others have shown to be composed of filamentous organic structures<sup>48-51</sup>. During the secretory stage of amelogenesis, the continuous exocytosis of amelogenin dimers may then contribute to elongate ribbons already present in the calcium phosphate-rich milieu of the extracellular space. A more detailed analysis of developing enamel is warranted to verify this model avoiding EDTA or demineralization by strong acids which would disintegrate amelogenin nanoribbons.

Calcium ions are well known to promote self-assembly of biomolecules through ion bridges as seen in centrin, cadherin, calmodulin, laminin<sup>52-54</sup>. Calcium binding to rH174 by electrostatic

interactions was proposed by several studies and an average of 6.5 binding sites per molecules has been calculated<sup>55, 56</sup>. Calcium may act as counter ion for phosphate bridges or electrostatically associate itself to acidic residues. A detailed analysis including the use of amelogenins with mutated histidines or other possible candidates for ion bridge formation will be required to more clearly define the mechanisms that drive ion binding and ribbon assembly.

However, the concurrent dependence upon pH and specific ions indicates that self-assembly is linked to protonation of residue side chains that mediate phosphate and/or calcium binding. Sequence and structural conservation analyses (mfsCa and mfsPO4) identified only glutamic and aspartic acid residues with a high probability of interaction with calcium, and predominantly histidines for phosphate (Figure 4B). The pKa's of these residues coincide with the shifts in self-assembly observed here. The acidic residues deprotonate around the pH 1.5 to 3.7, possibly causing the disintegration of self-assembled ribbons as observed at pH below 4 (Figure 2e). Histidines will be protonated at the lower pH range. While not widely studied in biominerization, numerous critical roles are described for histidine-phosphate interactions in kinase biology<sup>57</sup>. A recent study demonstrated biomineral interactions for peptides including the residues proposed here, having been identified by analogous informatic analyses of a predicted amelogenin structure and hydroxyapatite-binding sequences from phage display data evolutionary selection experiments<sup>58</sup>. Specifically, the histidine-rich regions were the only ones to interact with hydroxyapatite, while the acid-rich regions bound strongly to calcium. A better understanding of the roles of histidine and acidic residues in calcium and phosphate interactions may be crucial to produce a complete model of amelogenin self-assembly and

control over crystal growth. Using SAXS measurements on filtered suspensions, we observed that dimers become more abundant in the presence of calcium and phosphate when the pH is raised from acidic (pH 1.5) to pH 4.5 and become the dominant subunit structure at pH 5.6 and higher. The formation of dimers in suspensions of full-length amelogenin has been described by others and may not require calcium and phosphate ions<sup>42</sup>. Here we hypothesize that under our experimental conditions amelogenin is surrounded by a cloud of tightly associate calcium and phosphate ions preventing the monomer from folding by hydrophobic forces as the pH is raised from 2 to between 4 and 6, when protonated histidines can still bind phosphate. As a consequence, stable dimers are observed with a consistent SAXS profile enabling determination of a molecular surface outline for amelogenin (Figure 5B).

We constructed a multi-scale molecular model of amelogenin self-assembly by integrating the data from this study (Figure 6). SAXS and TEM data indicate overlapping of the molecules by about 75% in rH174 dimers (Supplementary Table). Hence all fourteen histidine residues of rH174 will be within the overlap zone. In our model the phosphate ions are in association with histidines. Interestingly their location also coincides with the ribbon center and the dark central line that is observed along the backbone of the amelogenin nanoribbons<sup>25</sup>. The line may thus originate from the high electron density of calcium and phosphorous atoms (Figure 6). Dimers are composed of molecules in antiparallel configuration with the hydrophilic C-terminus oriented towards the ribbon's edges. Hence electrostatic charges build at the edges and give rise to electrostatic repulsion of amelogenin nanoribbons ultimately causing their parallel alignment as predicted in our previous analysis<sup>25</sup>. The tendency to self-align was not observed on ribbons made from rH146 which lack the hydrophilic ends<sup>24</sup>. This also suggests that the observed

1  
2  
3 alignment of rH174 ribbons is not an artifact of specimen dehydration for TEM and AFM  
4 analysis. The alignment of ribbons ultimately leads to the formation of bundles composed of  
5 aligned ribbons (Fig. 1 D-G). Such bundles could, with the involvement of the ameloblasts,  
6 evolve into an organic precursor of the enamel rod ready for templating the formation of oriented  
7 apatite crystallization.  
8  
9  
10  
11  
12  
13

14  
15  
16  
17 We observed that amelogenin nanospheres become unstable in the presence of both calcium and  
18 phosphate ions. Others have also shown that monomers and oligomers co-exists with  
19 nanospheres and nanospheres readily release oligomers when in contact with solid surfaces<sup>59-61</sup>.  
20  
21 A recent publication reported on the hierarchical assembly of amelogenin nanospheres in the  
22 absence of calcium and phosphate ions, illustrating that such nanospheres completely  
23 disappeared when calcium and phosphate were added and mineralization was initiated<sup>11</sup>. Other  
24 studies were also not able to show evidence of nanosphere formation once apatite mineralization  
25 occurred, further supporting our finding that amelogenin nanospheres are unstable in solutions  
26 containing mineralizing ions<sup>18, 23</sup>.  
27  
28  
29  
30  
31  
32  
33  
34  
35  
36  
37

38  
39  
40 While it has been shown previously that divalent anions like HPO<sub>4</sub><sup>2-</sup> can act as bridges between  
41 peptide and protein molecules<sup>62</sup>, the mechanism of assembly by ion interaction with protonated  
42 histidine as shown in this study is novel. We have observed apatite crystallization in the presence  
43 of amelogenin nanoribbons. However, the formation of such crystals was not in association with  
44 the protein template, suggesting that the ribbons themselves may not act as apatite nucleator but  
45 perhaps as a reservoir of these ions. Moreover, we observed the presence of amorphous calcium  
46 phosphate in or around bundles of ribbons (Figure S4). This finding is in agreement with the  
47  
48  
49  
50  
51  
52  
53  
54  
55  
56  
57  
58  
59  
60

process of biomineralization, since as a common principle the secreted matrix does not induce mineralization directly without post-secretory modification (e.g. phosphorylation, proteolysis)<sup>63, 64</sup>. Interaction with other, non-amelogenin proteins or processing of amelogenin which are crucial to enamel formation may also be required for apatite crystallization and will be subject to future studies<sup>65</sup>.

## CONCLUSIONS

The formation of highly organized apatite crystals in dental enamel suggests that the organic matrix acts as a guide and template for mineral formation during tissue development. Here we developed a system that facilitated the formation of amelogenin nanoribbons in aqueous suspensions and describe the required physical-chemical parameters. In the presence of calcium and phosphate amelogenin nanospheres become unstable and disintegrate while gradually ribbons of specific width develop over a period of days, self-align and self-organize into micrometer sized bundles of ribbons. Ribbons of similar size and shape with a high degree of parallel alignment have been characterized by TEM analysis of the developing matrix of dental enamel<sup>48</sup>. Ribbon-like structures are part of many descriptions of the matrix of developing enamel<sup>49-51</sup>. The ability of amelogenin to form ribbons which develop into micrometer-sized bundles of aligned ribbons substantially impacts the current paradigm of amelogenin-guided mineralization of apatite in enamel and will provide critical insights into our understanding of amelogenesis as well as enhance our ability to generate enamel *in vitro* through biomimetic approaches.

## Acknowledgement

1  
2  
3 Dr. Stefan Duhr (NanoTemper Technologies) for facilitating the use of the MST system;  
4 Tsutomu Matsui, Lester Carter and Hiro Tsuruta at Stanford Synchrotron Radiation Lightsource  
5 for their support. NIH/NIDCR for financial support through RO1-DE017529, DE017529S2 and  
6 F30-DE017522 (J. A. Horst).  
7  
8  
9

10  
11 **Supporting Information Available:** a) SAXS data b) TEM images of control samples,  
12 including SAED of bundles of nanoribbons, c) Precision recall plot of MFS analysis. This  
13 material is available free of charge via the Internet at <http://pubs.acs.org>.  
14  
15

## 16 Figure Captions 17

20 **Figure 1.** TEM analysis of self-assembled structures of rH174 (0.4 mg/mL) observed at pH 4.5.  
21 (A) in the absence of calcium and phosphate ions at day 1 and (B) day 7 (C-H) compared to  
22 structures which develop over the same time period in the presence of calcium and phosphate:  
23 (C) day 1, shows both nanospheres and nanoribbons; (D) day 4, short ribbons of about 200-800  
24 nm length are the only structural feature observed; (E) day 5, domains of aligned ribbons appear;  
25 (F and G) day 7, bundle-like structures containing numerous aligned ribbons appear; (H) high-  
26 resolution of (G) showing that shorter ribbon segments are present at the end of the ribbons and  
27 in process to be added to existing longer and aligned ribbons; I) ribbons exposed to 0.5 M EDTA  
28 for 2h at pH 6, showing disintegration of ribbons, resulting in the appearance of nanospheres.  
29  
30

31 **Figure 2.** TEM and AFM images of supramolecular structures of rH174 at day 7 self-assembled  
32 at different pH. (A) pH 4.0, showing short randomly oriented ribbons; (B) pH 5.5 and C) pH 6.0  
33 ribbons have aligned and formed bundles. AFM images of (D) amelogenin nanoribbons formed  
34 at pH 4.5 and immobilized onto glass slide; E) same ribbons after rinsing with HCl-solution at  
35 pH 2, causing the ribbons to disintegrate; F) ribbons remained unchanged when exposed to  
36 buffered solutions at pH 7.0 for three days.  
37  
38

39 **Figure 3.** TEM images of supramolecular structures of rH174 present at day 6, as a function of  
40 protein concentration at pH 4.5: (A) at 0.4 mg/mL; (B) at 0.8 mg/mL; (C) at 1.2 mg/mL and (D)  
41 at 1.6 mg/mL. Size and alignment including the formation of bundles are enhanced with  
42 increasing protein concentration.  
43  
44

45 **Figure 4.** Structural binding analysis of amelogenin (H175) to calcium and phosphate ions. (A)  
46 Microscale Thermophoresis (MST) experiments show a strong change in fluorescence intensity  
47 in the presence of calcium and phosphate ions when unlabeled rH174 is titrated into labeled  
48 rH174 sols at pH 4.5 (black curve); indicating strong protein-protein interaction. The change in  
49 fluorescence was not quantifiable in the absence of calcium and phosphate (red data points). (B)  
50 Meta-functional signatures (MFS) showing the probability for each residue in amelogenin H175  
51 to bind soluble phosphate ions (mfsPO4) or soluble calcium ions (mfsCa). Scores above  
52 threshold (horizontal line) indicate high binding probability. Threshold was set at least three  
53 standard deviations higher than the mean for all scores of non-calcium or non-phosphate binding.  
54  
55

56 **Figure 5.**  
57  
58  
59  
60

Figure 5. Multiscale modeling of amelogenin ribbon assembly. *Ab-initio* shapes of (A) the rH174 monomer (cyan and yellow;  $R_g$  46.4 Å,  $D_{max}$  158 Å) and (B) rH174 dimer (gray wire;  $R_g$  64.1 Å,  $D_{max}$  209 Å) were derived from SAXS profiles measured in the presence of calcium and phosphate at pH 1.5 and pH 5.6, respectively. (B) Superimposition of SAXS-derived rH174 monomers within a rH174 dimer supports antiparallel symmetry (cross correlation coefficient = 0.82). (C) Antiparallel monomer orientation is also supported by comparison of an rH146 dimer (solid gray) superposed to an H174 dimer ( $CCC = 0.76$ ), which also reveals the carboxy termini lying on the distant ends of the H174 dimer. (D), (E) Building out these dimers as units of a multimer into a flat columnar template derived from TEM and AFM measurements of the ribbons presents a mechanistic molecular model of amelogenin self-assembly.

**Figure 6.** Comparison of the dimer-based model to a consensus TEM overlay for amelogenin nanoribbons. The apparent repeating units observed by TEM overlay are supported by the size and shape of the SAXS dimer model. The electron dense negative stain shown in the TEM, obtained in a previous study<sup>25</sup>, suggests buildup of calcium and phosphate along the center of the ribbon. Thus phosphates (orange) and histidines thought to carry out the pH dependent phosphate interactions are shown at the intersection of this region, with calcium ions (green) interspersed to represent potential counter ions for phosphate bridging. The coarse localization for histidines provides probabilistic tethers for future modeling efforts. The stacked orientation of amelogenin, calcium, and phosphate facilitates an explanation for the linear scaling of multimerization observed in this study. The SAXS based models of dimeric building blocks exceed the width of the ribbon as observed in the TEM by about 2 nm on both sides, suggesting that the non-overlapping portion at the C-terminus may be folded inwards.

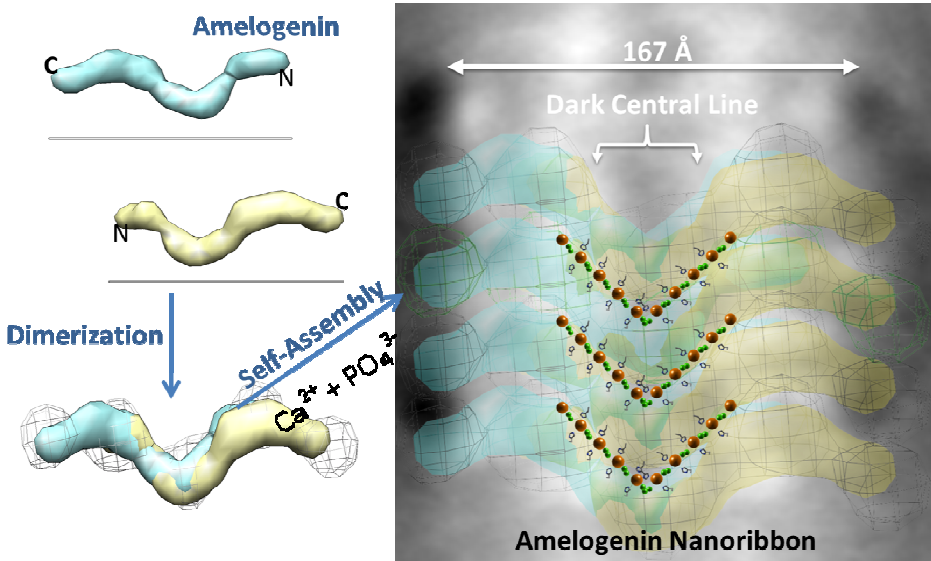
## REFERENCES

- (1) Smith, K. H.; Tejeda-Montes, E.; Poch, M.; Mata, A. *Chem. Soc. Rev.* **2011**, *40*, 4563-4577.
- (2) Ingber, D. E. *Sci. Am.* **1998**, *278*, 48-57.
- (3) Warshawsky, H. *Anat. Rec.* **1989**, *224*, 242-262.
- (4) White, S. N.; Luo, W.; Paine, M. L.; Fong, H.; Sarikaya, M.; Snead, M. L. *J. Dent. Res.* **2001**, *80*, 321-326.
- (5) Smith, C. E. *Crit. Rev. Oral Biol. Med.* **1998**, *9*, 128-161.
- (6) Fincham, A. G.; Moradian-Oldak, J.; Simmer, J. P. *J. Struct. Biol.* **1999**, *126*, 270-299.
- (7) Gibson, C. W.; Yuan, Z. A.; Hall, B.; Longenecker, G.; Chen, E.; Thyagarajan, T.; Sreenath, T.; Wright, J. T.; Decker, S.; Piddington, R.; Harrison, G.; Kulkarni, A. B. *J. Biol. Chem.* **2001**, *276*, 31871-31875.
- (8) Paine, M. L.; White, S. N.; Luo, W.; Fong, H.; Sarikaya, M.; Snead, M. L. *Matrix Biol.* **2001**, *20*, 273-292.
- (9) Moradian-Oldak, J. *Matrix Biol.* **2001**, *20*, 293-305.
- (10) Margolis, H. C.; Beniash, E.; Fowler, C. E. *J. Dent. Res.* **2006**, *85*, 775-793.
- (11) Fang, P. A.; Conway, J. F.; Margolis, H. C.; Simmer, J. P.; Beniash, E. *Proc. Natl. Acad. Sci. U.S.A.* **2011**, *108*, 14097-14102.

- (12) Delak, K.; Harcup, C.; Lakshminarayanan, R.; Sun, Z.; Fan, Y.; Moradian-Oldak, J.; Evans, J. S. *Biochemistry* **2009**, *48*, 2272-2281.
- (13) Lakshminarayanan, R.; Fan, D.; Du, C.; Moradian-Oldak, J. *Biophys. J.* **2007**, *93*, 3664-3674.
- (14) Du, C.; Falini, G.; Fermani, S.; Abbott, C.; Moradian-Oldak, J. *Science* **2005**, *307*, 1450-1454. Erratum in: *Science*. 2005 Sep 30;309(5744):2166
- (15) Zhang, X.; Ramirez, B. E.; Liao, X.; Diekwiisch, T. G. *PLoS One* **2011**, *6*, e24952.
- (16) Uskokovic, V.; Castiglione, Z.; Cubas, P.; Zhu, L.; Li, W.; Habelitz, S. *J. Dent. Res.* **2010**, *89*, 149-153.
- (17) Aichmayer, B.; Wiedemann-Bidlack, F. B.; Gilow, C.; Simmer, J. P.; Yamakoshi, Y.; Emmerling, F.; Margolis, H. C.; Fratzl, P. *Biomacromolecules* **2010**, *11*, 369-376.
- (18) Beniash, E.; Simmer, J. P.; Margolis, H. C. *J. Struct. Biol.* **2005**, *149*, 182-190.
- (19) He, X.; Li, W.; Habelitz, S. *J. Struct. Biol.* **2008**, *164*, 314-321.
- (20) Habelitz, S.; Kullar, A.; Marshall, S. J.; DenBesten, P. K.; Balooch, M.; Marshall, G. W.; Li, W. *J. Dent. Res.* **2004**, *83*, 698-702.
- (21) Lakshminarayanan, R.; Yoon, I.; Hegde, B. G.; Fan, D.; Du, C.; Moradian-Oldak, J. *Proteins* **2009**, *76*, 560-569.
- (22) Aichmayer, B.; Margolis, H. C.; Sigel, R.; Yamakoshi, Y.; Simmer, J. P.; Fratzl, P. *J Struct. Biol.* **2005**, *151*, 239-249.
- (23) Wiedemann-Bidlack, F. B.; Beniash, E.; Yamakoshi, Y.; Simmer, J. P.; Margolis, H. C. *J. Struct. Biol.* **2007**, *160*, 57-69.
- (24) Martinez-Avila, O. M.; Wu, S.; Cheng, Y.; Lee, R.; Khan, F.; Habelitz, S. *Eur. J. Oral Sci.* **2011**, *119 Suppl. 1*, 75-82.
- (25) He, X. D.; Wu, S. P.; Martinez-Avila, O.; Cheng, Y. F.; Habelitz, S. *J. Struct. Biol.* **2011**, *174*, 203-212.
- (26) Li, W.; Gao, C.; Yan, Y.; DenBesten, P. *Arch Oral Biol* **2003**, *48*, 177-183.
- (27) Bernado, P.; Modig, K.; Grela, P.; Svergun, D. I.; Tchorzewski, M.; Pons, M.; Akke, M. *Biophys. J.* **2010**, *98*, 2374-2382.
- (28) Svergun, D. I. *Biophys J* **1999**, *76*, 2879-2886.
- (29) Volkov, V. V.; Svergun, D. I. *J. Appl. Cryst.* **2003**, *36*, 860-864.
- (30) Pettersen, E. F.; Goddard, T. D.; Huang, C. C.; Couch, G. S.; Greenblatt, D. M.; Meng, E. C.; Ferrin, T. E. *J. Comput. Chem.* **2004**, *25*, 1605-1612.
- (31) Wang, K.; Horst, J. A.; Cheng, G.; Nickle, D. C.; Samudrala, R. *PLoS computational biology* **2008**, *4*, e1000181.
- (32) Horst, J. A.; Samudrala, R. *Pattern recognition letters* **2010**, *31*, 2103-2112.
- (33) Berman, H.; Henrick, K.; Nakamura, H.; Markley, J. L. *Nucleic Acids Res.* **2007**, *35*, D301-303.
- (34) Jerabek-Willemsen, M.; Wienken, C. J.; Braun, D.; Baaske, P.; Duhr, S. *Assay Drug Dev. Technol.* **2011**, *9*, 342-353.
- (35) Wienken, C. J.; Baaske, P.; Rothbauer, U.; Braun, D.; Duhr, S. *Nat. Commun* **2010**, *1*, 100.
- (36) Rosenberg, K.; Olsson, H.; Morgelin, M.; Heinegard, D. *J. Biol. Chem.* **1998**, *273*, 20397-20403.
- (37) Hiller, D. A.; Perona, J. J. *Biochemistry* **2006**, *45*, 11453-11463.
- (38) Ghanam, R. H.; Fernandez, T. F.; Fledderman, E. L.; Saad, J. S. *J. Biol. Chem.* **285**, 41911-41920.

- 1  
2  
3 (39) Stryer, L., *Biochemistry*. 4th ed.; W.H. Freeman & Company: 1995.  
4 (40) Glatter, O.; Kratky, O., *Small Angle X-ray Scattering*. Academic Press: 1982.  
5 (41) Matsushima, N.; Izumi, Y.; Aoba, T. *J. biochem.* **1998**, *123*, 150-156.  
6 (42) Buchko, G. W.; Tarasevich, B. J.; Bekhazi, J.; Snead, M. L.; Shaw, W. J. *Biochem.* **2008**,  
7 47, 13215-13222.  
8 (43) Bromley, K. M.; Kiss, A. S.; Lokappa, S. B.; Lakshminarayanan, R.; Fan, D.; Ndao, M.;  
9 Evans, J. S.; Moradian-Oldak, J., *J. biol. Chem.* **2011**, *286*, 34643-34653.  
10 (44) Aoba, T.; Moreno, E. C. *Calcif. Tissue Int.* **1987**, *41*, 86-94.  
11 (45) Lacruz, R. S.; Nanci, A.; Kurtz, I.; Wright, J. T.; Paine, M. L. *Calcif. Tissue Int.* **2010**, *86*,  
12 91-103.  
13 (46) Paroutis, P.; Touret, N.; Grinstein, S. *Physiology (Bethesda)* **2004**, *19*, 207-215.  
14 (47) Nanci, A.; Zalzal, S.; Lavoie, P.; Kunikata, M.; Chen, W.; Krebsbach, P. H.; Yamada, Y.;  
15 Hammarstrom, L.; Simmer, J. P.; Fincham, A. G.; Snead, M. L.; Smith, C. E. *J Histochem.*  
16 *Cytochem.* **1998**, *46*, 911-934.  
17 (48) Travis, D. F.; Glimcher, M. J. *J. Cell Biol.* **1964**, *23*, 447-497.  
18 (49) Diekwiisch, T. G. *Connect. Tissue Res.* **1998**, *38*, 101-111.  
19 (50) Nanci, A.; Bendayan, M.; Slavkin, H. C. *J Histochem. Cytochem.* **1985**, *33*, 1153-1160.  
20 (51) Meyer, J. M.; Bodier-Houelle, P.; Cuisinier, F. J.; Lesot, H.; Ruch, J. V. *In Vitro Cell Dev.*  
21 *Biol. Anim.* **1999**, *35*, 159-168.  
22 (52) Yurchenco, P. D.; Cheng, Y. S. *J. Biol. Chem.* **1993**, *268*, 17286-17299.  
23 (53) Alattia, J. R.; Ames, J. B.; Porumb, T.; Tong, K. I.; Heng, Y. M.; Ottensmeyer, P.; Kay, C.  
24 M.; Ikura, M. *FEBS Lett.* **1997**, *417*, 405-408.  
25 (54) Williams, R. J. *Cell calcium* **1992**, *13*, 355-362.  
26 (55) Le, T. Q.; Gochin, M.; Featherstone, J. D.; Li, W.; DenBesten, P. K. *Eur. J. Oral Sci.* **2006**,  
27 *114 Suppl. 1*, 320-326.  
28 (56) Uskokovic, V.; Li, W.; Habelitz, S. *J. Cryst. Growth* **2011**, *316*, 106-117.  
29 (57) Besant, P. G.; Attwood, P. V. *Biochim. Biophys. Acta* **2005**, *1754*, 281-290.  
30 (58) Gungormus, M.; Oren, E. E.; Horst, J. A.; Fong, H.; Hnilova, M.; Somerman, M. J.; Snead,  
31 M. L.; Samudrala, R.; Tamerler, C.; Sarikaya, M. *Int. J. Oral Sci.* **2012**, *4*, 69-77.  
32 (59) Tarasevich, B. J.; Lea, S.; Bernt, W.; Engelhard, M.; Shaw, W. J. *J. Physical Chem. B*  
33 **2009**, *113*, 1833-1842.  
34 (60) Tarasevich, B. J.; Lea, S.; Bernt, W.; Engelhard, M. H.; Shaw, W. J. *Biopolymers* **2009**,  
35 *91*, 103-107.  
36 (61) Chen, C. L.; Bromley, K. M.; Moradian-Oldak, J.; DeYoreo, J. J. *J. Am. Chem. Soc.* **2011**,  
37 *133*, 17406-17413.  
38 (62) Zou, D.; Tie, Z.; Lu, C.; Qin, M.; Lu, X.; Wang, M.; Wang, W.; Chen, P. *Biopolymers* **2010**,  
39 *93*, 318-329.  
40 (63) George, A.; Veis, A. *Chem. Rev.* **2008**, *108*, 4670-4693.  
41 (64) Qin, C.; Baba, O.; Butler, W. T. *Crit. Rev. Oral. Biol. Med.* **2004**, *15*, 126-136.  
42 (65) Smith, C. E.; Wazen, R.; Hu, Y.; Zalzal, S. F.; Nanci, A.; Simmer, J. P.; Hu, J. C. *Eur. J. Oral*  
43 *Sci.* **2009**, *117*, 485-497.  
44  
45  
46  
47  
48  
49  
50  
51  
52  
53  
54  
55  
56  
57  
58  
59  
60

TOC-Graphic:



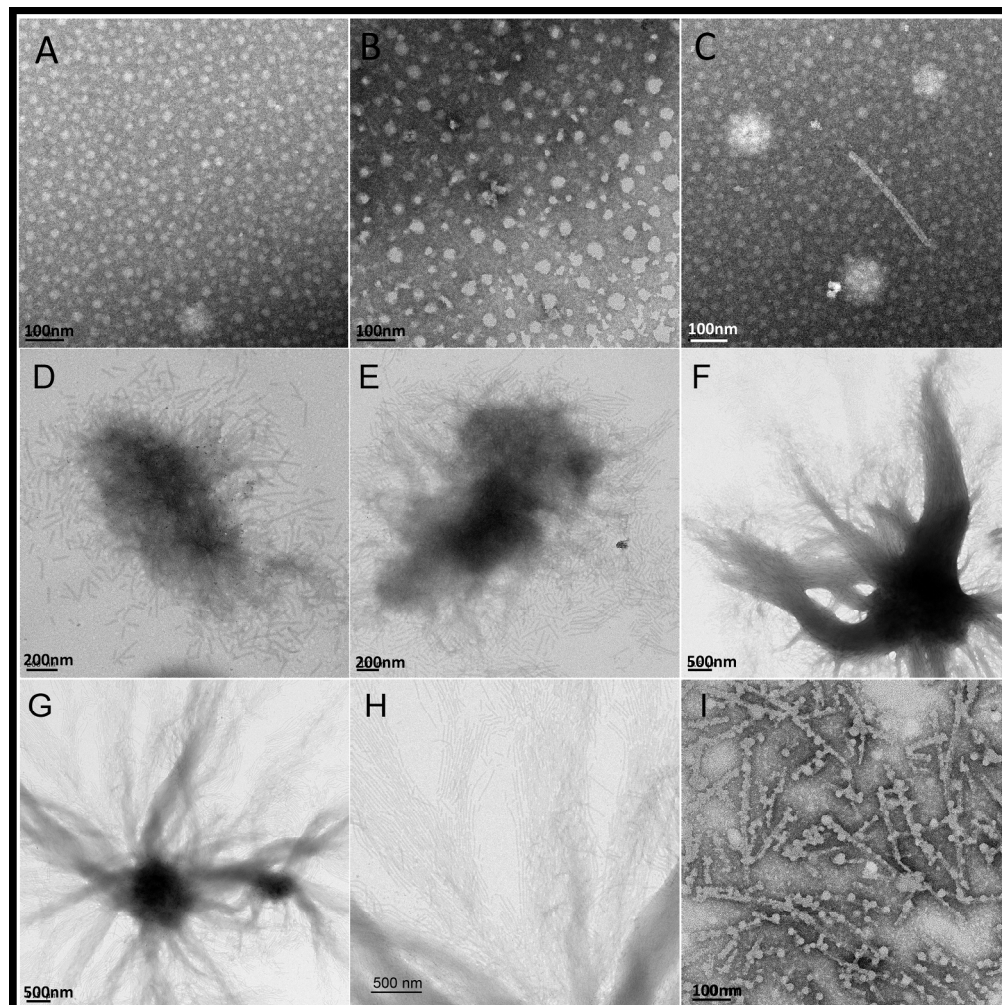


Figure 1. TEM analysis of self-assembled structures of rH174 (0.4 mg/mL) observed at pH 4.5. (A) in the absence of calcium and phosphate ions at day 1 and (B) day 7 (C-H) compared to structures which develop over the same time period in the presence of calcium and phosphate: (C) day 1, shows both nanospheres and nanoribbons; (D) day 4, short ribbons of about 200-800 nm length are the only structural feature observed; (E) day 5, domains of aligned ribbons appear; (F and G) day 7, bundle-like structures containing numerous aligned ribbons appear; (H) high-resolution of (G) showing that shorter ribbon segments are present at the end of the ribbons and in process to be added to existing longer and aligned ribbons; I) ribbons exposed to 0.5 M EDTA for 2 h at pH 6, showing disintegration of ribbons, resulting in the appearance of nanospheres.  
478x480mm (150 x 150 DPI)

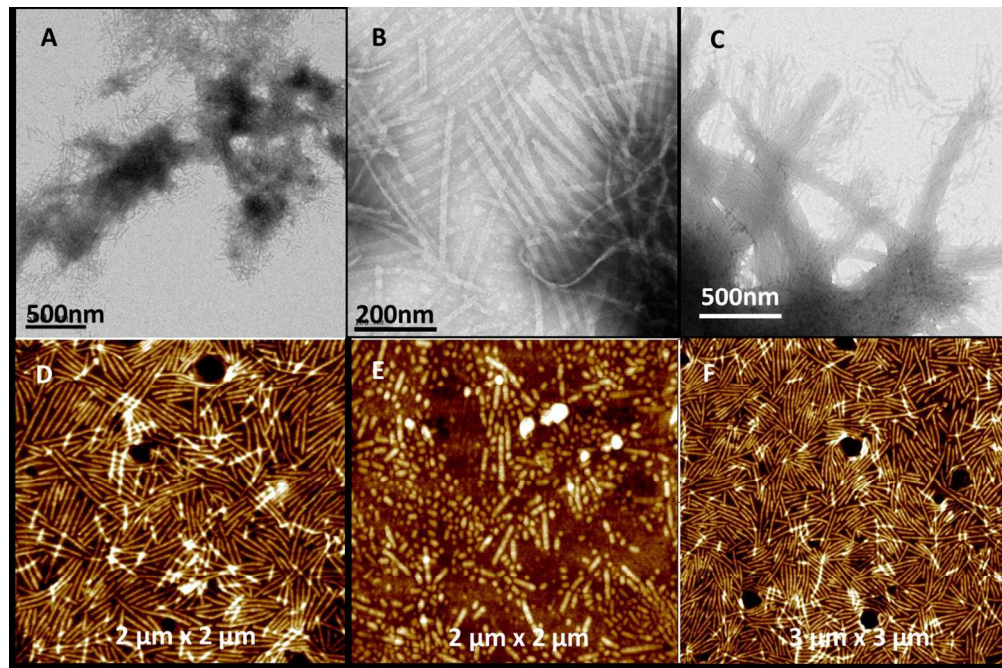


Figure 2. TEM and AFM images of supramolecular structures of rH174 at day 7 self-assembled at different pH. (A) pH 4.0, showing short randomly oriented ribbons; (B) pH 5.51 and C) pH 6.0 ribbons have aligned and formed bundles. AFM images of (D) amelogenin nanoribbons formed at pH 4.5 and immobilized onto glass slide; E) same ribbons after rinsing with HCl-solution at pH 2, causing the ribbons to disintegrate; F) ribbons remained unchanged when exposed to buffered solutions at pH 7.0 for three days.

231x153mm (150 x 150 DPI)

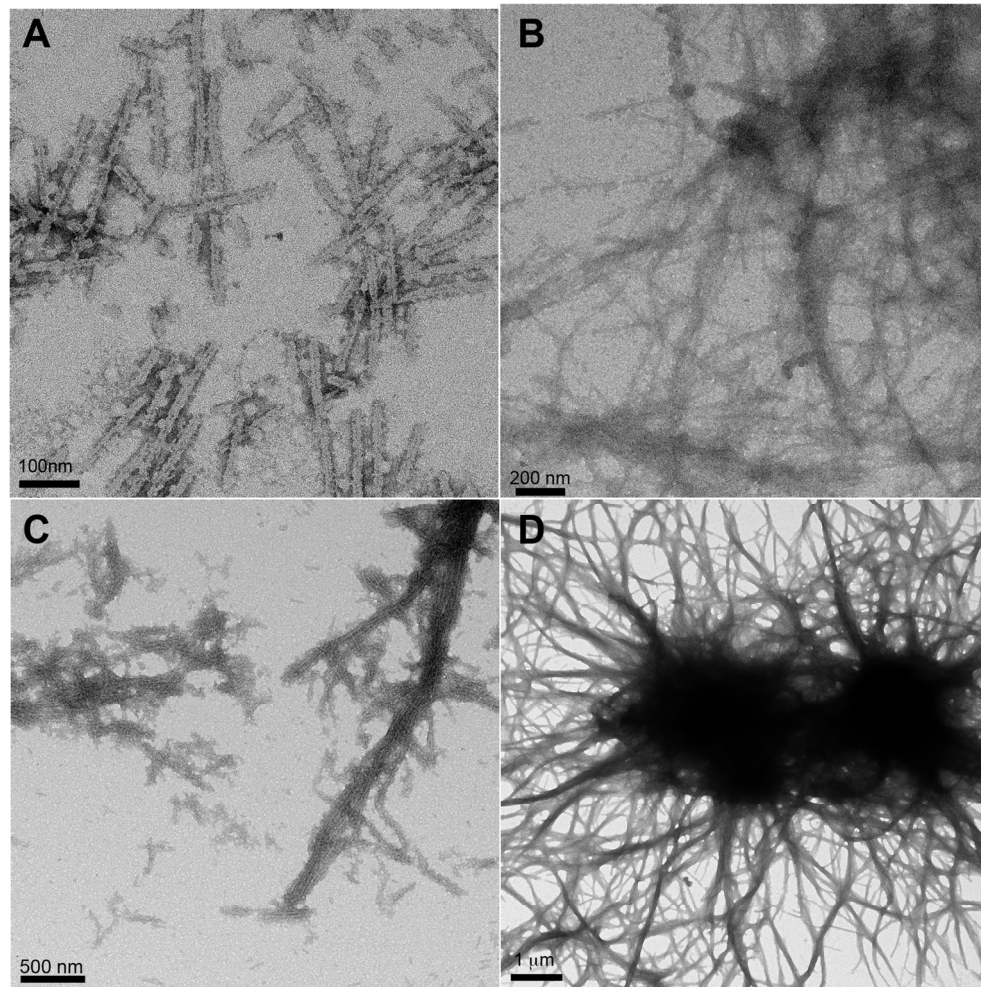


Figure 3. TEM images of supramolecular structures of rH174 present at day 6, as a function of protein concentration: (A) at 0.4 mg/mL; (B) at 0.8 mg/mL; (C) at 1.2 mg/mL and (D) at 1.6 mg/mL. Size and alignment including the formation of bundles are enhanced with increasing protein concentration.

304x304mm (150 x 150 DPI)

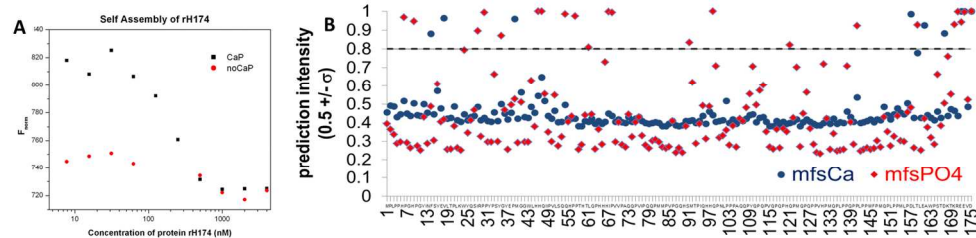


Figure 4. Structural binding analysis of amelogenin (H175) to calcium and phosphate ions. (A) Microscale Thermophoresis (MST) experiments show a strong change in fluorescence intensity in the presence of calcium and phosphate ions when unlabeled rH174 is titrated into labeled rH174 sols at pH 4.5 (black curve); indicating strong protein-protein interaction. The change in fluorescence was not quantifiable in the absence of calcium and phosphate (red data points). (B) Meta-functional signatures (MFS) showing the probability for each residue in amelogenin H175 to bind soluble phosphate ions (mfsPO<sub>4</sub>) or soluble calcium ions (mfsCa). Scores above threshold (horizontal line) indicate high binding probability. Threshold was set at least three standard deviations higher than the mean for all scores of non-calcium or non-phosphate binding.

304x76mm (150 x 150 DPI)

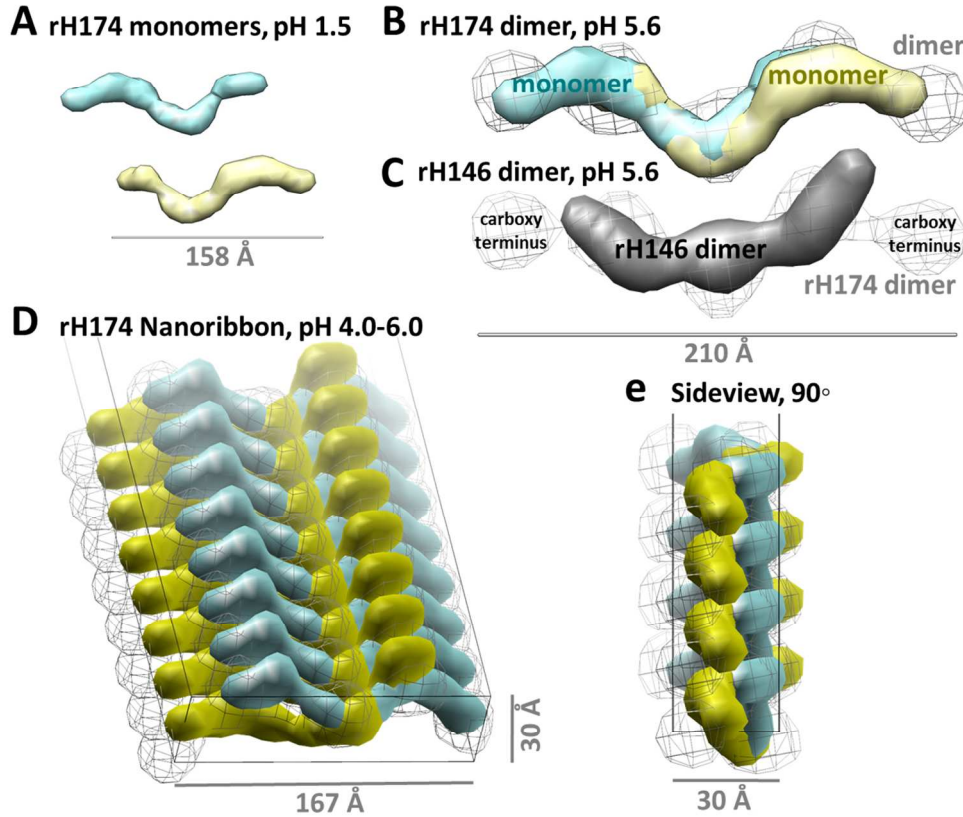


Figure 5.

Figure 5. Multiscale modeling of amelogenin ribbon assembly. Ab-initio shapes of (A) the rH174 monomer (cyan and yellow;  $R_g$  46.4 Å,  $D_{max}$  158 Å) and (B) rH174 dimer (gray wire;  $R_g$  64.1 Å,  $D_{max}$  209 Å) were derived from SAXS profiles measured in the presence of calcium and phosphate at pH 1.5 and pH 5.6, respectively. (B) Superimposition of SAXS-derived rH174 monomers within a rH174 dimer supports antiparallel symmetry (cross correlation coefficient = 0.82). (C) Antiparallel monomer orientation is also supported by comparison of an rH146 dimer (solid gray) superposed to an H174 dimer ( $CCC = 0.76$ ), which also reveals the carboxy termini lying on the distant ends of the H174 dimer. (D), (E) Building out these dimers as units of a multimer into a flat columnar template derived from TEM and AFM measurements of the ribbons presents a mechanistic molecular model of amelogenin self-assembly.

217x186mm (150 x 150 DPI)

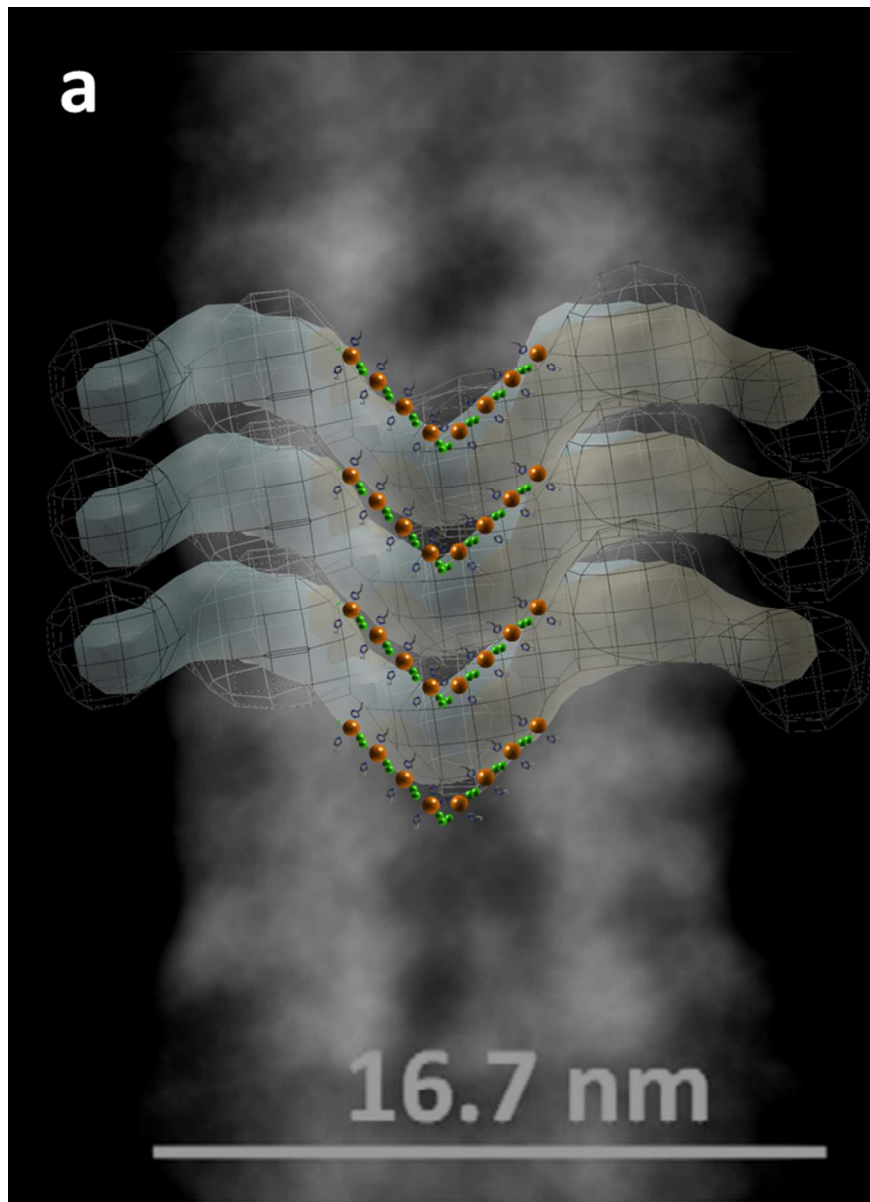


Figure 6. Overlay of the dimer-based amelogenin nanoribbon model over rH174 observed by TEM. Electron dense atoms, e.g. calcium and phosphorus, were aligned with positions of ionic bonds to histidine residues along the interface between amelogenin molecules. The location of mineralizing ions matched the central dark line observed in amelogenin nanoribbons by TEM 25 creating the ribbon structure of amelogenin assemblies of dimers. The SAXS based models of dimeric building blocks exceed the width of the ribbon as observed in the TEM by about 2nm on both sides.

124x171mm (150 x 150 DPI)